Variable Macro X Domain of SARS-CoV-2 Retains the Ability to Bind ADP-ribose

David N. Frick,[1]* Rajdeep S. Virdi,[1] Nemanja Vuksanovic,[1] Narayan Dahal,[2] & Nicholas R. Silvaggi[1]

Departments of Chemistry & Biochemistry,[1] and Physics,[2] The University of Wisconsin- Milwaukee, Milwaukee, WI 53217

KEYWORDS: COVID-19, Antiviral Drug target, Severe Acute Respiratory Syndrome, Coronavirus.

Supporting Information Placeholder

ABSTRACT: The virus that causes COVID-19, SARS-CoV-2, has a large RNA genome that encodes numerous proteins that might be targets for antiviral drugs. Some of these proteins, such as the RNA-dependent RNA polymers, helicase and main protease, are well conserved between SARS-CoV-2 and the original SARS virus, but several others are not. This study examines one of the most novel proteins encoded by SARS-CoV-2, a macrodomain of nonstructural protein 3 (nsp3). Although 26% of the amino acids in this SARS-CoV-2 macrodomain differ from those seen in other coronaviruses, the protein retains the ability to bind ADP-ribose, which is an important characteristic of beta coronaviruses, and potential therapeutic target.

The development of antivirals targeting Severe Acute Respiratory Syndrome Coronavirus 2 (SARS-CoV-2), the causative agent of the present COVID-19 pandemic,[1] will most likely focus on viral proteins and enzymes needed for replication.[2] Like other coronaviruses, SARS-CoV-2 has a large positive sense (+)RNA genome over 30,000 nucleotides long with several open reading frames. Most of the proteins that form the viral replicase are encoded by the "rep 1ab" reading frame, which codes for a 7,096 amino acid-long polyprotein that is ultimately processed into at least 15 functional peptides, five of which are only produced by a translational frameshift event occurring after nsp10 (Fig. 1). Parts of the SARS-CoV-2 rep 1ab polyprotein are very similar to the rep 1ab protein of the coronavirus that caused the SARS epidemic in 2003 (which will be referred to here as SARS-CoV-1), suggesting the that drugs targeting the SARS-CoV-1 nsp5-14 might be effective against SARS-CoV-2. However, some portions of the SARS rep 1ab polyproteins are quite different.

In contrast to the well-conserved SARS nsp5 protease, nsp12 polymerase and nsp13 helicase enzymes, significantly more differences exist between the nsp3 proteins encoded by SARS-CoV-1 and SARS-CoV-2. The most variation occurs in a domain of Nsp3 domain suspected to bind ADP-ribose, that will be referred to here as the "macro X" domain, to differentiate it from the two downstream "SARS unique macrodomains (SUDs)," which do not bind ADP-ribose.[3] The macro X domain of SARS-CoV-1 is also able to catalyze the hydrolysis of ADP-ribose 1" phosphate, albeit at a slow rate.[4]

All the above differences preclude the use of the SARS-CoV-1 macro X domain structures as scaffolds to design compounds that might target this nsp3 region in SARS CoV-2, especially in light of the observation that the same nsp3 domain from gamma coronaviruses does not bind ADP-ribose *in vitro*.[5] Because ADP-ribose binding is a property that could be used to identify possible antiviral agents, the ability of the SARS-CoV-2 macro X domain to bind ADP-ribose was examined using a recombinant purified protein and isothermal titration calorimetry (ITC). We also determined the structure of the SARS-CoV-2 macro X domain in order to examine the biochemical context of ADP-ribose binding and to provide data for rational inhibitor design or *in silico* screening.

RESULTS AND DISCUSSION

Hypervariability in the nsp3 Macro X domain— The structures of most of the soluble portions of the SARS-CoV-1 nsp proteins have been examined at atomic resolution to help understand coronavirus replication and facilitate antiviral drug discovery. The amino acid sequences of each of these proteins were compared with the homologous regions of the rep 1ab protein encoded by SARS-CoV-2 (GenPept Accession YP_009724389). The most similar proteins were the RNA helicases (nsp13) which are identical in all but one of their 603 amino acids: a conservative Val to Ile substitution near their C-termini. The RNA-dependent RNA polymerases (nsp12) are also well-conserved, sharing all but 34 of 955 amino acids. The primary protease that cleaves the polyprotein (nsp5) is also similar in SARS-CoV-1 and SARS-CoV-2, with only 13 amino acids that differ among 306 (4.2% different) (Fig. 1).

At the other end of the spectrum are the nsp3 proteins, which are notably more different in the two SARS viruses. Nsp3 is a large multidomain membrane-bound protein,[6] and its clearest role in viral replication is cleaving the rep polyprotein. Over 17% of the amino acids in the nsp3 protease domain differ between SARS-CoV-1 and SARS-CoV-2. Other parts of nsp3 are even more variable, like the macrodomains that lie N-terminal to the nsp3 protease domain. Macrodomains consist of four helices that surround a mixed beta sheet. A ligand-binding pocket that typically binds ADP-ribose or related compounds lies between the helices and the sheet.[7] SARS-CoV-1 has three macrodomains in tandem, but only the first binds ADP ribose. The amino acid sequences of this macro X domain differ by 26% between SARS-CoV-1 and SARS-CoV-2 (Fig. 1).

Many of the 47 variant residues in the 180 amino acid long SARS macro X domain are clustered near its N-terminus in a region that is particularly variable in the three *Coronaviridae* genera (Fig. 2). Macro X domains from coronaviruses that cause the common cold (alpha coronaviruses)[5] and the beta coronaviruses like SARS-CoV-1 and Middle East respiratory syndrome coronavirus (MERS-CoV)[8] all bind ADP ribose. However, the same domain in gamma coronaviruses does not bind ADP-ribose.[5]

Expression and Purification of the SARS-CoV-2 Macro X domain— An *E. coli* expression vector for the macro X domain was built to express and N-terminally His-tagged protein similar to a SARS-CoV-1 protein studied by Egloff *et al.*[9] Upon induction, a one liter culture of BL21(DE3) cells harboring the vector expresses 50-100 mg of the macro X domain protein that can be purified in one step to apparent homogeneity using immobilized metal affinity chromatography (Fig. 3A).

Nucleotide Binding by the SARS-CoV-2 Macro X domain— Repeated ITC experiments revealed that the purified recombinant protein bound ADP-ribose (Fig. 3C) with a dissociation constant of 10 ± 4 μM (uncertainty is the standard deviation of K_d's from independent titrations). To examine binding specificity, similar titrations were repeated with related nucleotides. The SARS-CoV-2 protein bound ADP, cAMP, ATP and ADP-glucose (Fig. 3D). All nucleotides lacking the ribose moiety bound with similar high affinities, but none bound with an enthalpy change like that seen with ADP-ribose, suggesting specific contacts form between ADP ribose the SARS-CoV-2 protein. Based on what is seen in the SARS-CoV-2 structures below, these contacts likely occur with the conserved D226 and N244 (positions 30 and 43 in the numbering above the alignment in Fig. 2). None of the other nucleotides bind with an entropic penalty as seen with ADP-ribose, either, suggesting that the ribose moiety becomes structured when bound to the macrodomain.

The energetics of ADP-ribose binding to the SARS-CoV protein are similar to those seen with the same protein from SARS-CoV-1,[9] MERS-CoV.[8] Enthalpy and entropy of binding were also very similar for all three protein (Fig. 3D). Unlike what is seen with the macro X protein from an alpha coronavirus,[5] enthalpy appears to drive ADP-ribose binding to the macro X domains of the three beta coronaviruses.

Structure of the SARS-CoV-2 Macro X Domain— The SARS CoV-2 macro X domain (NSP3 residues 207 to 277) crystallized in space group $P2_12_12_1$ with 1 molecule per asymmetric unit. These crystals had a solvent content of 43% and diffracted extremely well. The final resolution limit of the data was set at 0.95 Å (Table 1). The quality of the electron density maps is correspondingly excellent (Fig. 4A). The section of the structure depicted in this image is located on the surface of the protein and the B-factors of these residues are close to the average B-factor of the protein (7.2 vs 10.2 $Å^2$), indicating that this sample accurately represents the overall quality of the maps. The final model contains the entire sequence from V207 to S377 of nsp3, an N-terminal glycine residue that was left from the TEV-protease cleavage, and 374 solvent molecules. The R_{cryst} and R_{free} values of the final model were 0.119 and 0.137, respectively (Table 1).

The tertiary structure, as expected, ranges from nearly identical to very similar to those of other coronavirus macro domains, including: SARS CoV-1 (2FAV[9]; 74.7% sequence identity) with a root mean square deviation (RMSD) value for 162 of 172 Cα atoms of 0.6 Å; MERS CoV (5DUS[8]; 42.2% identical) with a 1.2 Å RMSD for 161 of 172 Cα atoms; human alpha coronavirus 229E (3EWR[10]; 32.5% identical) with a 1.5 Å RMSD for 154 of 172 Cα atoms; feline coronavirus (FCoV; 3JZT[11] 26.8% identical) with a 1.5 Å RMSD for 153 of 172 Cα atoms; and the gamma CoV infectious bronchitis virus (IBV; 3EWP[10] 26.7% identical) with a 2.1 Å RMSD for 150 of 172 Cα atoms. The regions of high sequence conservation are not clustered in any particular region(s) of the molecule (Fig. 4B). This makes sense in light of the fact that the protein atoms involved in hydrogen bonding interactions with the ligands in these structures are more often part of the main chain; there are relatively few interactions of side chains with the ligands.

At the time of writing, we discovered that Michalska *et al.* of the Center for Structural Genomics of Infectious Diseases (CSGID) deposited coordinates for a very similar construct of the SARS-CoV-2 macro X domain including from E206 to E275 of the nsp3 protein, plus an additional 4 residues at the N-terminus (6VSX; unpublished). Their crystals also allowed binding of ADP-ribose (6W02) and AMP (6W6Y), while ours seemed to be packed too tightly to permit ligands to access the binding site (data not shown). We compared our ultra-high-resolution model of the unliganded protein to the ADP-ribose-bound form. The RMSD values for the fitting, done by secondary structure matching (SSM)[12] as implemented in COOT, is 0.59 Å for 165 of 172 Cα atoms. This is very

similar to the RMSD values of the free protein (6VXS; 0.66 Å) and the AMP-bound form (6W6Y; 0.50 Å), indicating that there are no large conformational changes that occur upon ligand binding. In fact, the only notable conformational changes occur in three surface-exposed loops in or near the ligand-binding pocket (Fig. 4C). These loops connect strand β2 with helix α2 (the β2-α2 loop), strand β4 with helix α4 (β4-α4 loop), and strand β5 with helix α5 (β5-α5 loop). The subtle change in conformation of the β4-α4 loop (purple in Fig. 4C) appears to be the result of crystal contacts and not the direct influence of ADP-ribose binding. The other two loops are more intimately involved in ligand binding. The main chain of the α2-β2 loop rotates 180° in order to allow the amide N atom of G252 to participate in a hydrogen bonding interaction with the 1'-hydroxyl of the ribose moiety of ADP-ribose. This loop also carries N244, which directly interacts with the ribose. The phenyl ring of F336 in the β5-α5 loop occupies the portion of the binding pocket in the unliganded structure that is occupied by the β-phosphate of ADP-ribose. Thus, without a rearrangement of the β5-α5 loop, ADP-ribose would not be able to bind.

Conclusion— The significance of the study stems mainly from the demonstration that the SARS-CoV-2 macro X domain binds ADP ribose. This is the first step needed to justify screens for potential antivirals that bind in place of ADP ribose. More work needs to be done, however, to understand the antiviral potential of such compounds because the biological role for ADP-ribose binding is still not fully understood. Some work with alpha coronaviruses suggest that ADP-ribose binding by the macro X domain is not needed for viral replication.[13] However, studies with other (+)RNA viruses suggest that macrodomains are essential for virulence.[14] This work is also noteworthy because the synthetic codon-optimized plasmid reported here produces up to 100 mg of soluble macro X domain protein per liter of *E. coli* culture, and this protein retains a high affinity for ADP ribose. The protein could be used for structural studies and screening campaigns. Screening assays with the SARS-CoV-2 protein might actually be more efficient, since the SARS-CoV-2 protein binds ADP-ribose somewhat more tightly (K_d = 10 μM) than the SARS-CoV-1 protein (K_d = 24 μM). The recombinant protein reported here, together with the detailed structural information, might also be useful to others developing SARS-CoV-2 diagnostics and/or therapeutics.

METHODS

Gene Synthesis— To facilitate comparison between SARS-CoV-1 and SARS-CoV-2, a protein expression vector was generated similar to the one used by Eglott *et al.*[9] To this end, a codon optimized open reading frame was synthesized by GenSript (Piscataway, NJ) that encodes the Macro X domain with an N-terminal TEV-cleavage site flanked by *Nhe*I and *Bam*H1 restriction sites. This open reading frame was cloned into pET21b to give plasmid pET21-COVID-MacroX. The pET11-COVID-MacroX plasmid was used to transform BL21(DE3) cells.

Protein Purification— Colonies of BL21(DE3) cells harboring the pET21-COVID-MacroX plasmid were used to inoculate 3 ml of LB medium containing 100 mg/ml ampicillin. The starter culture was incubated at 37 °C with shaking at 225 rpm. After the cells grew to an OD_{600} of 1.0, they were transferred to 1 liter of fresh medium containing ampicillin. After the cells reached an OD_{600} of 1.0 again, protein production was induced with 1 mM isopropyl-β-D-thiogalactoside. After growing 16 h at 23 °C, the cells were harvested by centrifugation at 4,000 rpm, 4°C. The resulting cell pellet was suspended in 25 mL of IMAC buffer (20 mM Tris pH 8, 0.5 M NaCl), sonicated on ice for five 1 min bursts, with 2 min rests between, and clarified by centrifugation at 10,000g for 30 min. The supernatant was loaded onto a 5 ml Ni-NTA column and the fractions were eluted with a step gradient from 5 to 500 mM imidazole. Fractions containing the macro X domain protein (5 ml total) were loaded on a 250 ml Sephacryl S300 gel filtration column and eluted with 10 mM MOPS, 150 mM NaCl. Concentration of the purified protein was determined by measuring absorbance at 260 nm using a molar extinction coefficient of 10,555 M^{-1} cm^{-1}, which was calculated with the ProtParam tool (https://web.expasy.org/protparam/).

Isothermal Titration Calorimetry (ITC)— Binding of ADP-ribose to the SARS-CoV-2 macro X domain was measured using a Nano ITC (TA Instruments). Before starting the measurement, samples of both ligand and protein were diluted in 10 mM MOPS, 150 mM NaCl (pH 7) and were degassed at 400 mmHg for 30 minutes. Measurements were taken at 20 °C by injecting 2.0 μl aliquots of 500 μM ADP-Ribose (Sigma) to 50 μM protein (175 μl initial volume) with 250 rpm stirring rate. Using NanoAnalyze Software (v. 3.11.0), data were fitted by non-linear regression to an independent binding model. Briefly, after baseline correction, background heats from ligand-to-buffer titrations were subtracted, and the corrected heats from the binding reaction were used to find best fit parameters for the stoichiometry of the binding (n), free energy of binding (ΔG), apparent enthalpy of binding (ΔH), and entropy change (ΔS). Dissociation constants (K_d) were calculated from the ΔG.

Crystallization and Structure Determination— In preparation for crystallization experiments, the purified SARS-CoV-2 macro X domain protein was cleaved with tobacco etch virus (TEV) protease to remove the N-terminal His_6-tag and passed back through the Ni-NTA column. The flow-through fractions were desalted into 10 mM HEPES, pH 7.2 using a 2x5ml HiTrap desalting column (GE Life Sciences) and concentrated to 10 mg/mL in a centrifugal concentrator. This preparation of the protein was mixed 1 μL:1 μL with the Morpheus HT screen reagents (Molecular Dimensions) in a 96-well SwissSci

MRC UV-transmissible sitting drop plate. Large, diffraction-quality crystals grew directly from a number of the screen conditions. The crystal ultimately used for structure determination grew from condition D9: 0.12 M alcohols [0.02 M each 1,6-hexanediol, 1-butanol, 1,2-propanediol, 2-propanol, 1,4-butanediol, and 1,3-propanediol], 0.1 M buffer system 3, pH 8.5 [0.05 M each TRIS and bicine], and 30% precipitant mix 1 [20% poly(ethylene glycol) (PEG) 500 monomethylether, 10% PEG 20,000]. Large, thick plates grew within 1 week at 22 °C. Owing to the high concentration of PEG 500 MME, the crystal did not require additional cryo-protection and was flash-cooled by looping it directly from the sitting drop and plunging it into liquid nitrogen.

Diffraction data were collected on Life Sciences Collaborative Access Team (LS-CAT) beamline 21-ID-F at the Advanced Photon Source of Argonne National Laboratory. The wavelength at this station is fixed at 0.9787 Å; the detector is a MarMosaic M300 charge-coupled device. The data were collected with an oscillation width of 0.5° per image for a total oscillation of 180°. The data were indexed and integrated with DIALS [15, 16] as implemented in version 7.2 of the CCP4 software suite.[17, 18] Data scaling and reduction was performed using AIMLESS.[19–21] Data collection statistics are provided in Table 1.

The structure was determined by molecular replacement in PHASER[22] using the model of the SARS-CoV-1 macro X domain as the search model (PDB ID 2FAV[9]). The model underwent iterative rounds of (re)building in COOT[23] and refinement in PHENIX.refine.[24, 25] The very high resolution of the data justified a full anisotropic treatment of the protein and solvent temperature factors. Model refinement and validation statistics are provided in Table 1. The coordinates were deposited in the Protein Data Bank with accession code 6WEY.

Corresponding Author

*(D.N.F.) Phone: (414) 229-6670. Fax: (414) 229-5530. E-mail: frickd@uwm.edu.

Funding Sources

No competing financial interests have been declared.

ACKNOWLEDGMENTS

The authors are grateful to Matt McCarty, Garrett Breit, Hayden Aristizabal, Trevor R. Melkonian, Dante A. Serrano and Prof. Ionel Popa for valuable technical assistance and helpful discussions.

This research used resources of the Advanced Photon Source, a U.S. Department of Energy (DOE) Office of Science User Facility operated for the DOE Office of Science by Argonne National Laboratory under Contract No. DE-AC02-06CH11357. Use of the LS-CAT Sector 21 was supported by the Michigan Economic Development Corporation and the Michigan Technology Tri-Corridor (Grant 085P1000817).

REFERENCES

1. Wu F, Zhao S, Yu B, Chen YM, Wang W, Song ZG, Hu Y, Tao ZW, Tian JH, Pei YY, Yuan ML, Zhang YL, Dai FH, Liu Y, Wang QM, Zheng JJ, Xu L, Holmes EC, Zhang YZ. A new coronavirus associated with human respiratory disease in China. Nature 2020;579:265-269.
2. Subissi L, Imbert I, Ferron F, Collet A, Coutard B, Decroly E, Canard B. SARS-CoV ORF1b-encoded nonstructural proteins 12-16: replicative enzymes as antiviral targets. Antiviral Res 2014;101:122-130.
3. Kusov Y, Tan J, Alvarez E, Enjuanes L, Hilgenfeld R. A G-quadruplex-binding macrodomain within the "SARS-unique domain" is essential for the activity of the SARS-coronavirus replication-transcription complex. Virology 2015;484:313-322.
4. Saikatendu KS, Joseph JS, Subramanian V, Clayton T, Griffith M, Moy K, Velasquez J, Neuman BW, Buchmeier MJ, Stevens RC, Kuhn P. Structural basis of severe acute respiratory syndrome coronavirus ADP-ribose-1''-phosphate dephosphorylation by a conserved domain of nsP3. Structure 2005;13:1665-1675.
5. Piotrowski Y, Hansen G, Boomaars-van der Zanden AL, Snijder EJ, Gorbalenya AE, Hilgenfeld R. Crystal structures of the X-domains of a Group-1 and a Group-3 coronavirus reveal that ADP-ribose-binding may not be a conserved property. Protein Sci 2009;18:6-16.
6. Lei J, Kusov Y, Hilgenfeld R. Nsp3 of coronaviruses: Structures and functions of a large multi-domain protein. Antiviral Res 2018;149:58-74.
7. Leung AKL, McPherson RL, Griffin DE. Macrodomain ADP-ribosylhydrolase and the pathogenesis of infectious diseases. PLoS Pathog 2018;14:e1006864.
8. Cho CC, Lin MH, Chuang CY, Hsu CH. Macro Domain from Middle East Respiratory Syndrome Coronavirus (MERS-CoV) Is an Efficient ADP-ribose Binding Module: CRYSTAL STRUCTURE AND BIOCHEMICAL STUDIES. J Biol Chem 2016;291:4894-4902.
9. Egloff MP, Malet H, Putics A, Heinonen M, Dutartre H, Frangeul A, Gruez A, Campanacci V, Cambillau C, Ziebuhr J, Ahola T, Canard B. Structural and functional basis for ADP-ribose and poly(ADP-ribose) binding by viral macro domains. J Virol 2006;80:8493-8502.
10. Xu Y, Cong L, Chen C, Wei L, Zhao Q, Xu X, Ma Y, Bartlam M, Rao Z. Crystal structures of two coronavirus ADP-ribose-1''-monophosphatases and their complexes with ADP-Ribose: a systematic structural analysis of the viral ADRP domain. J Virol 2009;83:1083-1092.
11. Wojdyla JA, Manolaridis I, Snijder EJ, Gorbalenya AE, Coutard B, Piotrowski Y, Hilgenfeld R, Tucker PA. Structure of the X (ADRP) domain of nsp3 from feline coronavirus. Acta Crystallogr D Biol Crystallogr 2009;65:1292-1300.
12. Krissinel E, Henrick K. Secondary-structure matching (SSM), a new tool for fast protein structure alignment in three dimensions. Acta Crystallogr D Biol Crystallogr 2004;60:2256-2268.
13. Keep S, Bickerton E, Armesto M, Britton P. The ADRP domain from a virulent strain of infectious bronchitis virus is not sufficient to confer a pathogenic phenotype to the attenuated Beaudette strain. J Gen Virol 2018;99:1097-1102.
14. Abraham R, McPherson RL, Dasovich M, Badiee M, Leung AKL, Griffin DE. Both ADP-Ribosyl-Binding and Hydrolase Activities of the Alphavirus nsP3 Macrodomain Affect Neurovirulence in Mice. mBio 2020;11
15. Clabbers MTB, Gruene T, Parkhurst JM, Abrahams JP, Waterman DG. Electron diffraction data processing with DIALS. Acta Crystallogr D Struct Biol 2018;74:506-518.
16. Winter G, Waterman DG, Parkhurst JM, Brewster AS, Gildea RJ, Gerstel M, Fuentes-Montero L, Vollmar M, Michels-Clark T, Young ID, Sauter NK, Evans G. DIALS: implementation and evaluation of a new integration package. Acta Crystallogr D Struct Biol 2018;74:85-97.

17. Winn MD, Ballard CC, Cowtan KD, Dodson EJ, Emsley P, Evans PR, Keegan RM, Krissinel EB, Leslie AG, McCoy A, McNicholas SJ, Murshudov GN, Pannu NS, Potterton EA, Powell HR, Read RJ, Vagin A, Wilson KS. Overview of the CCP4 suite and current developments. Acta Crystallogr D Biol Crystallogr 2011;67:235-242.

18. Potterton L, Agirre J, Ballard C, Cowtan K, Dodson E, Evans PR, Jenkins HT, Keegan R, Krissinel E, Stevenson K, Lebedev A, McNicholas SJ, Nicholls RA, Noble M, Pannu NS, Roth C, Sheldrick G, Skubak P, Turkenburg J, Uski V, von Delft F, Waterman D, Wilson K, Winn M, Wojdyr M. CCP4i2: the new graphical user interface to the CCP4 program suite. Acta Crystallogr D Struct Biol 2018;74:68-84.

19. Evans PR, Murshudov GN. How good are my data and what is the resolution. Acta Crystallogr D Biol Crystallogr 2013;69:1204-1214.

20. Evans P. Scaling and assessment of data quality. Acta Crystallogr D Biol Crystallogr 2006;62:72-82.

21. Evans PR. An introduction to data reduction: space-group determination, scaling and intensity statistics. Acta Crystallogr D Biol Crystallogr 2011;67:282-292.

22. McCoy AJ, Grosse-Kunstleve RW, Adams PD, Winn MD, Storoni LC, Read RJ. Phaser crystallographic software. J Appl Crystallogr 2007;40:658-674.

23. Emsley P, Lohkamp B, Scott WG, Cowtan K. Features and development of Coot. Acta Crystallogr D Biol Crystallogr 2010;66:486-501.

24. Liebschner D, Afonine PV, Baker ML, Bunkóczi G, Chen VB, Croll TI, Hintze B, Hung LW, Jain S, McCoy AJ, Moriarty NW, Oeffner RD, Poon BK, Prisant MG, Read RJ, Richardson JS, Richardson DC, Sammito MD, Sobolev OV, Stockwell DH, Terwilliger TC, Urzhumtsev AG, Videau LL, Williams CJ, Adams PD. Macromolecular structure determination using X-rays, neutrons and electrons: recent developments in Phenix. Acta Crystallogr D Struct Biol 2019;75:861-877.

25. Afonine PV, Grosse-Kunstleve RW, Echols N, Headd JJ, Moriarty NW, Mustyakimov M, Terwilliger TC, Urzhumtsev A, Zwart PH, Adams PD. Towards automated crystallographic structure refinement with phenix.refine. Acta Crystallogr D Biol Crystallogr 2012;68:352-367.

26. Almeida MS, Johnson MA, Herrmann T, Geralt M, Wüthrich K. Novel beta-barrel fold in the nuclear magnetic resonance structure of the replicase nonstructural protein 1 from the severe acute respiratory syndrome coronavirus. J Virol 2007;81:3151-3161.

27. Johnson MA, Chatterjee A, Neuman BW, Wüthrich K. SARS coronavirus unique domain: three-domain molecular architecture in solution and RNA binding. J Mol Biol 2010;400:724-742.

28. Báez-Santos YM, Barraza SJ, Wilson MW, Agius MP, Mielech AM, Davis NM, Baker SC, Larsen SD, Mesecar AD. X-ray structural and biological evaluation of a series of potent and highly selective inhibitors of human coronavirus papain-like proteases. J Med Chem 2014;57:2393-2412.

29. Serrano P, Johnson MA, Chatterjee A, Neuman BW, Joseph JS, Buchmeier MJ, Kuhn P, Wüthrich K. Nuclear magnetic resonance structure of the nucleic acid-binding domain of severe acute respiratory syndrome coronavirus nonstructural protein 3. J Virol 2009;83:12998-13008.

30. Akaji K, Konno H, Mitsui H, Teruya K, Shimamoto Y, Hattori Y, Ozaki T, Kusunoki M, Sanjoh A. Structure-based design, synthesis, and evaluation of peptide-mimetic SARS 3CL protease inhibitors. J Med Chem 2011;54:7962-7973.

31. Kirchdoerfer RN, Ward AB. Structure of the SARS-CoV nsp12 polymerase bound to nsp7 and nsp8 co-factors. Nat Commun 2019;10:2342.

32. Egloff MP, Ferron F, Campanacci V, Longhi S, Rancurel C, Dutartre H, Snijder EJ, Gorbalenya AE, Cambillau C, Canard B. The severe acute respiratory syndrome-coronavirus replicative protein nsp9 is a single-stranded RNA-binding subunit unique in the RNA virus world. Proc Natl Acad Sci U S A 2004;101:3792-3796.

33. Ma Y, Wu L, Shaw N, Gao Y, Wang J, Sun Y, Lou Z, Yan L, Zhang R, Rao Z. Structural basis and functional analysis of the SARS coronavirus nsp14-nsp10 complex. Proc Natl Acad Sci U S A 2015;112:9436-9441.

34. Jia Z, Yan L, Ren Z, Wu L, Wang J, Guo J, Zheng L, Ming Z, Zhang L, Lou Z, Rao Z. Delicate structural coordination of the Severe Acute Respiratory Syndrome coronavirus Nsp13 upon ATP hydrolysis. Nucleic Acids Res 2019;47:6538-6550.

35. Ricagno S, Egloff MP, Ulferts R, Coutard B, Nurizzo D, Campanacci V, Cambillau C, Ziebuhr J, Canard B. Crystal structure and mechanistic determinants of SARS coronavirus nonstructural protein 15 define an endoribonuclease family. Proc Natl Acad Sci U S A 2006;103:11892-11897.

36. Decroly E, Debarnot C, Ferron F, Bouvet M, Coutard B, Imbert I, Gluais L, Papageorgiou N, Sharff A, Bricogne G, Ortiz-Lombardia M, Lescar J, Canard B. Crystal structure and functional analysis of the SARS-coronavirus RNA cap 2'-O-methyltransferase nsp10/nsp16 complex. PLoS Pathog 2011;7:e1002059.

37. Pettersen EF, Goddard TD, Huang CC, Couch GS, Greenblatt DM, Meng EC, Ferrin TE. UCSF Chimera--a visualization system for exploratory research and analysis. J Comput Chem 2004;25:1605-1612.

Table 1. Crystallographic data collection and model refinement statistics for the SARS-CoV-2 Macro X domain.

Data collection	
Resolution range (Å) (last shell)[a]	43.32 – 0.95 (0.97 – 0.95)
Space Group	P 2_1 2_1 2_1
***a*, *b*, *c* (Å)**	43.3, 54.4, 67.6
α, β, γ (°)	90.0, 90.0, 90.0
R_{merge}[a]	0.063 (0.348)
R_{meas}[a]	0.075 (0.475)
R_{pim}[a]	0.039 (0.320)
$CC_{1/2}$[a]	99.5 (89.1)
No. of unique reflections[a]	99442 (4199)
Completeness (%)[a]	98.4 (85.0)
Multiplicity[a]	6.4 (2.6)
$\langle I/\sigma(I)\rangle$[a]	13.1 (1.5)
Model Refinement	
Reflections used in refinement	99335 (2606)[b]
Reflections used for R_{free}	5046 (125)
R_{cryst} (R_{free})	0.119 (0.137)
Wilson B-factor (Å^2)	7.4
Average B factor (Å^2)	13.9
Protein atoms	10.2
Solvent	28.2
Root-mean-square (RMS) deviations	
Bond lengths (Å)	0.010
Bond angles (°)	1.16
Coordinate error (Å)	0.06
Ramachandran statistics	
Favored/allowed/outliers (%)	98.2/1.8/0.0
Rotamer outliers (%)	1.2
Clashscore	1.70

[a]Values in parentheses apply to the high-resolution shell indicated in the resolution row

[b]The limits of the high-resolution bin for refinement were 0.96 – 0.95Å

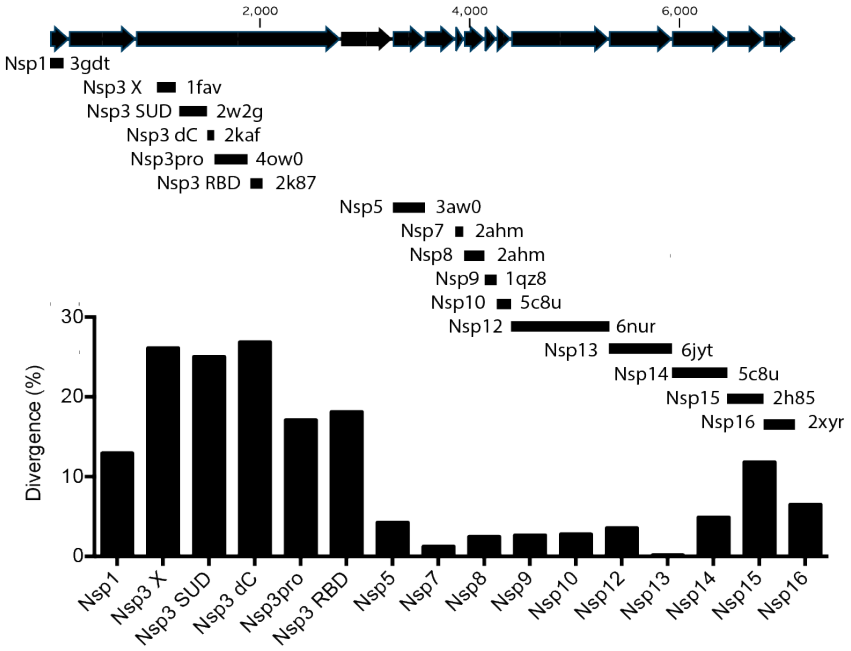

FIGURE 1. **Sequence divergence between potential drug targets in SARS-CoV-1 and SARS-CoV-2.** The SARS-CoV-2 rep 1ab peptide sequence was aligned with each of the PDB files listed, which describe an atomic structure of a homologous region of the SARS-CoV-1 rep 1ab polyprotein. Nsp's are shown in sequence as black arrows (note: there is no "nsp11", and the translational frameshift occurs after nsp10). The percent of amino that differ in each protein is plotted. For details see Fig. S1 (supporting information). Nsp1 is and interferon antagonist.[26] The Nsp3 X domain is studied here, the Nsp3 SUD consists of tandem macrodomains that bind G-quadruplex structures,[3] Nsp dC is the C-terminus of the SUD,[27] Nsp3pro is a papain-like protease,[28] and Nsp3 RBD is another possible RNA binding domain.[29] Nsp5 is the main viral protease.[30] Nsp7 and Nsp8 are polymerase cofactors.[31] Nsp9 is an RNA binding protein.[32] Nsp10 is a zinc-binding cofactor for Nsp14 and Nsp16.[33] Nsp12 is the RNA polymerase.[31] Nsp13 is a helicase.[34] Nsp14 is a 3'-5' exonuclease and a 7-methyltransferase.[33] Nsp15 is an RNA endonuclease.[35] Nsp16 is an RNA cap 2'-O-Methyltransferase.[36]

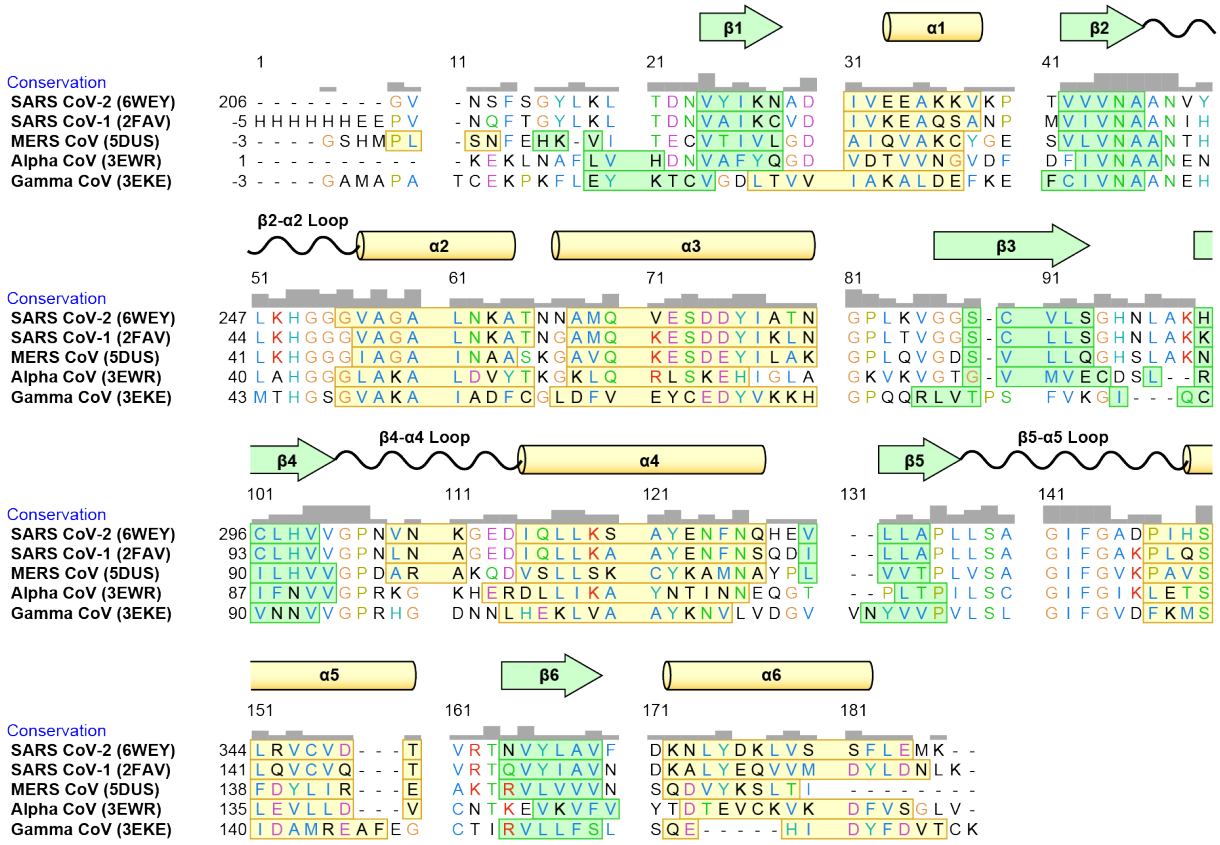

FIGURE 2. **Variation in the macro X domains of coronaviruses.** (A) Macro X domain structures were aligned using the "MatchMaker" function of UCSF Chimera (v. 1.14).[37] Amino acids are colored by class with beta sheets in green boxes and alpha helices in yellow boxes.

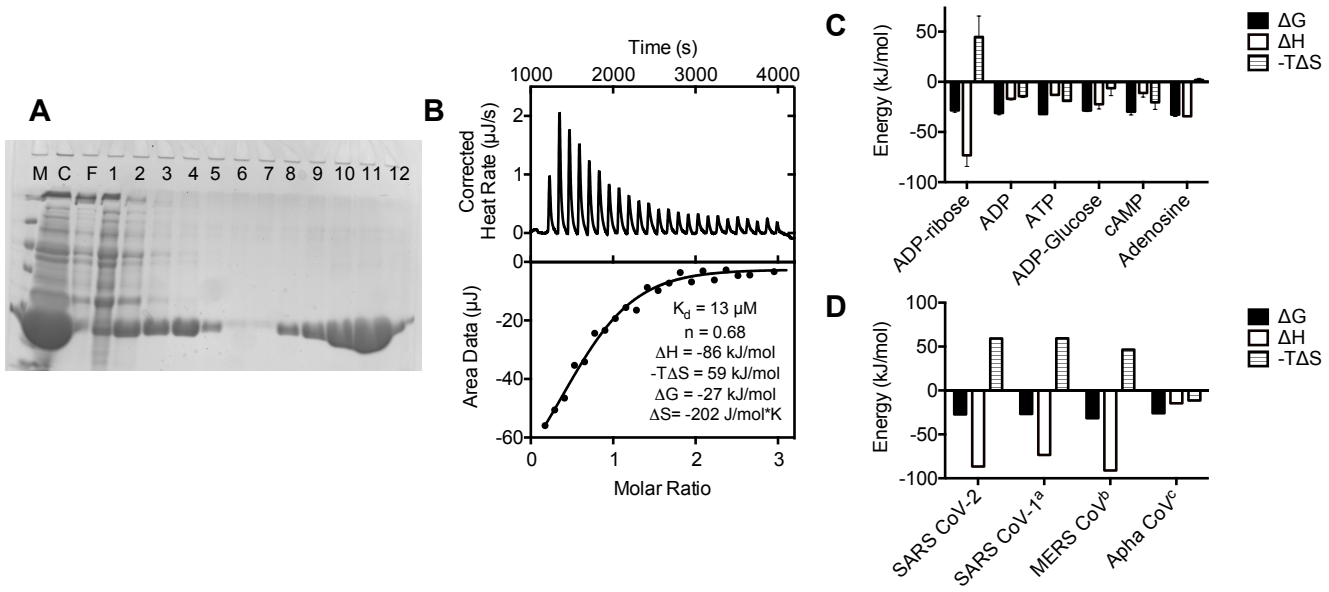

FIGURE 3. **The SARS-CoV-2 macro X domain binds ADP ribose.** (A) 15% SDS PAGE showing 10 µL samples of: a soluble crude lysate of induced BL21(DE3) cells harboring the plasmid p21-COVID-MacroX (lane C), proteins the do not bind a Ni-NTA column (F), and fractions eluted from a NiNTA column during an imidazole step gradient from 0 mM (lanes 1-3), 5 mM (lanes 4-6), 40 mM (lanes 7-9), and 500 mM (lanes 10-12). Protein markers (lane M) are 116, 66.2, 45, 35, and 25 kDa. (B) Example ITC experiment in which purified SARS-CoV-2 was titrated with ADP ribose. (C) ITC experiments like those shown in panel B were repeated tree times with each of the compounds listed. Means are plotted and error bars are standard deviations. Average (±SD) dissociation constants were 10 ± 4 µM for ADP-ribose, 8 ± 9 µM for ADP, 3 ± 3 µM for ATP, 6± 4 µM for ADP-glucose, 2 ± 1 µM for cAMP, and 2 ± 1 µM for adenosine. (D) Comparison of the thermodynamics of ADP-ribose binding by macro X domains from SARS-CoV-2 (data from panel C), SARS-CoV-1, MERS-CoV, and an alpha coronavirus. [a]Data from Egloff et al.[32] [b]Data from Cho et al.[8] [c]Data from Piotrowski et al.[5]

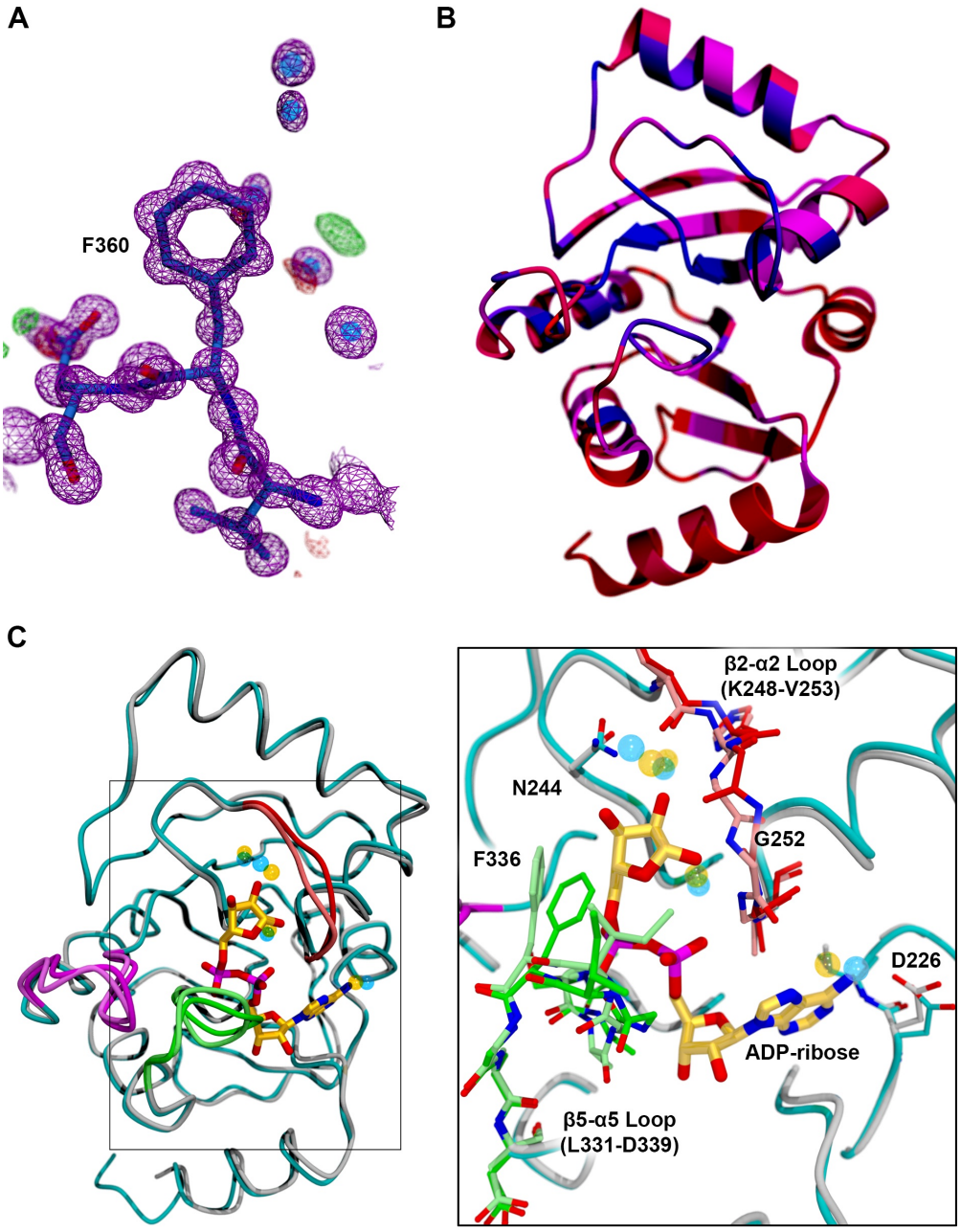

FIGURE 4. **The SARS-CoV-2 macro X domain structure.** (A) The electron density is shown for a representative portion of the structure (residues 359-361) on the surface of the protein. The $2mF_o$-DF_c map is contoured at 1.5σ and is shown as a magenta mesh. The mF_o-DF_c (difference) maps are shown at + and – 3.0σ as green and red mesh, respectively. (B) Ribbon diagram of the SARS-CoV-2 macro X domain structure colored according to the sequence conservation plot in Figure 2 as a gradient from red (low conservation; <10%) to blue (highly conserved; 100%) through magenta. As can be seen in the sequence alignment, the N- and C-termini are particularly poorly conserved. (C) Overlay of the structure of the SARS-CoV-2 macro X domain bound to ADP-ribose determined by Michalska *et al*. of the CGSID (PDB ID 6W02) with the ultra-high-resolution structure of the unliganded protein determined here. ADP-ribose is shown in ball-and-stick with the carbon atoms colored gold. The backbone trace of the unliganded structure is colored cyan, and that of the ADP-ribose-bound model is colored grey. There are three loops with significantly different conformations in the two structures. In the unliganded structure, the β2-α2 loop is colored bright red, the β4-α4 loop is colored purple, and the β5-α5 loop is colored bright green. The same regions of the ADP-ribose-bound structure are colored pale red, pale purple, and pale green, respectively. The transparent blue and yellow spheres represent water molecules bound to the unliganded (transparent blue) and ADP-ribose-bound (transparent yellow) forms of the protein. Interestingly, several of the water molecules interacting with ADP-ribose in 6W02 can also be found in the unliganded structure of the protein. The inset shows a close-up of the boxed region colored according to the same scheme. The β2-α2 and β5-α5 loops, which contact ADP-ribose, are shown in ball-and-stick. Note that the β2-α2 loop rotates ~180° to allow it to make a hydrogen-bonding interaction with the 1'-hydroxyl of the ribose moiety. Also, the phenylalanine residue in the β5-α5 loop (F336) would clash with the β-phosphate and ribose of ADP-ribose if the β5-α5 loop did not adopt a different conformation.

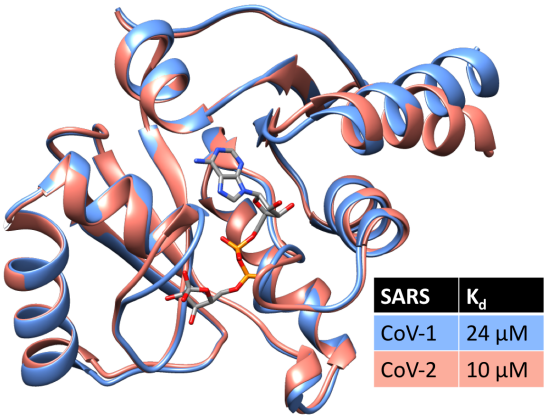
SARS
K_d
CoV-1
24 µM
CoV-2
10 µM